Contents list available at IJRED website

International Journal of Renewable Energy Development

Journal homepage: https://ijred.undip.ac.id

Research Article

Optimum Control of Grid-Connected Solar Power System Under Asymmetrical Voltage Drop

Van Binh Nguyen*

School of Electrical Engineering, International University, Vietnam National University, Ho Chi Minh City 700000, Viet Nam

Abstract. Solar power systems are now gradually dominating in providing clean, environmentally friendly energy and human health. In areas with a large share of solar power, grid connection control plays a key role in ensuring operational quality and stability, especially in the event of a grid failure. In case of asymmetrical voltage drop, the control system needs to maintain operation and create a function to assist in restoring the power grid. This study proposes a method to control the solar power system in the condition of asymmetric grid voltage drop based on the method of controlling symmetrical components. Controllers for each of the forward and inverse components are built to limit the effects of failures. The optimal control parameter calculation method is also proposed to improve the overall quality and minimize the undesired variation of the electromagnetic quantities. The simulation and experimental results are verified to evaluate the effectiveness of the grid-connected control method in converting DC power to three-phase power.

Keywords: Solar power, Grid connection control, Grid disturbance, Symmetrical component, Inverse sequence controller

Received: 8th March 2022; Revised: 13th May 2022; Accepted: 26th May 2022; Available online: 2th June 2022

1. Introduction

Renewable energy is currently being invested heavily in replacing fossil energy sources that are harmful to the environment and human health. Among clean energy sources, the production of clean electricity from solar energy has many advantages such as quick installation, less impact on the natural ecosystem. In addition, the solar system has a simple, safe structure, and it is easy to change the required capacity.

The solar power system collects energy from photovoltaic (PV) panels that generate direct current (Figure 1). The voltage and power obtained depends on the size of the investment and is fully adjustable during the operating process. The output power is controlled through a DC-DC converter. The optimal current with a radiation level is determined by the MPPT (Maximum Power Point Tracking) algorithm. The U_{DC} voltage is controlled through a DC-AC converter to achieve the required voltage level and convert all the power supplied to the grid. The LC-filter removes high-order harmonics due to the switching of semiconductor valves to generate a sine current in sync with the grid. For a distribution network with a high percentage of solar power, the grid connection control mechanism needs to meet national standards to maintain and support grid recovery when short-term problems occur.

For grid control in case of excess energy for fixed loads, many works have published solutions to connect this energy to the grid.

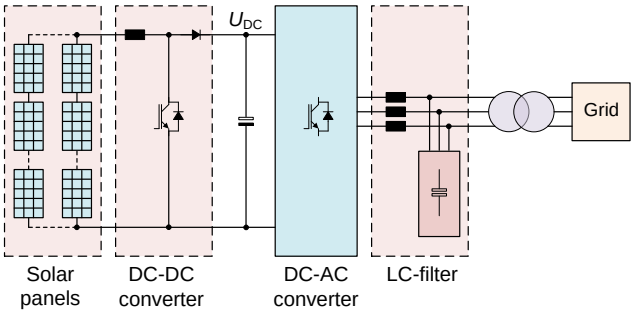

Fig. 1 Structure of solar power generation system

These solutions ensure voltage and frequency synchronization with different power electronic structures and control techniques (Kjaer *et al.*, 2005). Grid-tied solar PV system has received much attention with many contributions to different control techniques related to inverter stages, DC/DC and DC/AC conversion methods (Prakash *et al.*, 2015; Moghadasi *et al.*, 2017; Li *et al.*, 2012; Shao *et al.*, 2014; Zapata *et al.*, 2015; Dousoky *et al.*, 2013). Omar *et al.* (2021) presented a case study using simulation to find the optimal matching parameters of a PV array connected to an inverter. Various solar inverter topologies are also proposed with different approaches such as DC/AC converter (Sahu *et al.*, 2015), Flyback inverter (Kyritsis *et al.*, 2008; Zhang *et al.*, 2010; Nanakos *et al.*, 2012; Kim *et al.*, 2013; Lodh and Agarwal, 2016), forward microinverter (Gagrica *et al.*, 2015; Meneses *et al.*, 2015), cascaded H-

* Corresponding author:
Email: nvbinh@hcmiu.edu.vn

https://doi.org/10.14710/ijred.2022.45115
ISSN: 2252-4940/© 2022.The Author(s). Published by CBIORE

Bridge inverter (Chen *et al*., 2015; Coppola *et al*., 2016; Premkumar *et al*., 2018b), grid-interfaced filter based inverter (Zhu *et al*., 2015; Yashi *et al*., 2017). For other technology related to grid connection, Premkumar *et al*. (2018a) gives detailed review on different works for grid connected solar PV micro-inverter and suggests the reliable, suitable and efficient topologies for micro-inverter.

One of the most important issues today is to ensure that the solar system continues to generate real and reactive power during grid failure. Different countries have different standards for grid connectivity. Control techniques focus on two aspects, voltage drop on single-phase systems and symmetric/asymmetric three-phase voltage drop. In the case of symmetrical single-phase and three-phase voltage drops, grid recovery control can be done by adding reactive current to the grid (Yang *et al*., 2014). Control techniques in the case of symmetric voltage drop continue to be developed and make certain contributions (Vicuna *et al*., 2015; Tekpeti *et al*., 2017; Mohanty *et al*., 2019; Banu and Istrate, 2014).

In the asymmetric case, the control technique can be used according to the symmetrical three-phase components according to the direct and inverse rotation systems (Hajizadeh and Golkar, 2011; Wang *et al*., 2015). Hunter *et al*. (2019) presented an experimental implementation to obtain a real-time validation of a control strategy, intended to inject the desired active/reactive power during asymmetrical voltage sags and swells in a single-stage PV system. Related studies on the operation of the inverter under voltage unbalanced conditions were also proposed with different approaches. Castilla *et al*. (2010) explored the performance of PV inverters under unbalanced voltage sags. They proposed a control strategy based on the use of continuous values for the control parameters. Another work was introduced with a control algorithm for reference current generation that provides flexible voltage support under grid faults for three-phase inverters. (Camacho *et al*., 2013). Sosa *et al*. (2016) proposed a low-voltage ride-through control strategy that maximizes the inverter power capability by injecting the maximum-rated current during the sag. The control uses a flexible current injection strategy that combines a proper balance between forward and inverse current sequences, which limits the inverter output current to the maximum rated value and avoid active power oscillations. Other methods aim to reduce the DC-link voltage oscillations and currents injected to the grid during unsymmetrical voltage sag (Almeida *et al*., 2016; Ding *et al*., 2016; Miret *et al*., 2012; Lin *et al*., 2018). However, a general solution to the connectivity problem in case of grid failure still requires further research.

This study proposes a method to control the solar power system in the condition of grid voltage drop based on three phase symmetrical components. Optimal control parameters would be described for simultaneous control of important system parameters. Regarding the layout in the article, Section 2 presents grid connection standards, a new symmetrical component separation and system modelling. Next, the work presents an approach that uses the method of controlling the symmetric components in a three-phase system to ensure that the grid standards are maintained (Section 3). Section 4 proposes optimal control parameter determination and experimental results are shown to evaluate the feasibility of the method.

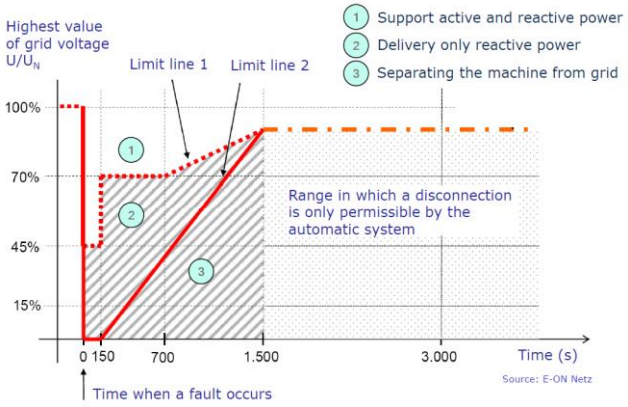

Fig. 2 Fault ride-through requirements of the E.ON grid code

2. Grid connection and system modelling

2.1 Grid connection standards

For large renewable energy power systems, which account for most of the electricity supplied to an area, the grid-connected controller needs to maintain connection in case the grid becomes unstable in a short time. For three-phase transmission or distribution power systems, the fault may occur on one or more phases. The cause may be short circuit, overload or starting large power machines. Depending on the type and location of the fault, the voltage drop can range from 10 to 90%. Failure times can range from 0.3 grid cycles to several seconds (Arrillaga *et al*., 2000). Common types of grid faults can be mentioned as three-phase voltage drop, single phase voltage drop, two phase voltage drop, single phase short circuit to ground, two phase short circuit. Currently, both amplitude and time of grid failures can be improved through protection solutions and fast response times of grid-connected control systems.

For countries with a large proportion of grid-connected electricity from solar or wind energy, the grid connection of generating systems needs to be ensured according to a common standard framework. Figure 2 describes a European standard fault recovery grid connection requirement (Erlich *et al*., 2006). According to this standard, when the voltage drop is above the limit line 1, the generator needs to be stable and stay connected to the grid, generating both active and reactive power. In the condition between the limit lines 1 and 2, the generator needs to generate a lot of reactive power to assist in grid recovery.

2.2 Symmetrical component representation

A symmetric component analysis can split an asymmetric three-phase system into two symmetric systems and a zero-order symmetric component. These two symmetric components with opposite rotation directions are called direct and inverse components. The formula for separating the components is described by Eq. (1).

$$\begin{pmatrix} \underline{z}_{1a} \\ \underline{z}_{2a} \\ \underline{z}_{0a} \end{pmatrix} = \frac{1}{3}\begin{pmatrix} 1 & \underline{a} & \underline{a}^2 \\ 1 & \underline{a}^2 & \underline{a} \\ 1 & 1 & 1 \end{pmatrix}\begin{pmatrix} z_a \\ z_b \\ z_c \end{pmatrix} \quad (1)$$

where $\underline{a} = e^{j2\pi/3}$. The direct component, denoted by the number 1 ($\underline{z}_{1a}$, $\underline{z}_{1b}$, $\underline{z}_{1c}$) has the sequence of phases a, b and c and the direction of rotation is the same as the original system ($\underline{z}_a$, $\underline{z}_b$, $\underline{z}_c$), while the inverse component, denoted by the number 2 ($\underline{z}_{2a}$, $\underline{z}_{2c}$, $\underline{z}_{2b}$) has the sequence of phases and the direction of rotation is opposite. Fig. 3 describes the composition of the direct rotation coordinate system d_1q_1 and the inverse rotation system d_2q_2.

2.3 Symmetrical component separation method

Most of the separation methods use filters or delays in order to split the direct and inverse components of the asymmetrical three-phase variables (Alepuz *et al*., 2007; Saccomando and Svensson, 2001). The filter based method is used under the fact that the direct sequence component is as the first harmonic on the positive coordinate meanwhile the inverse sequence component is as the second harmonic on the negative rotating frame (Figure 3). Therefore, a low-pass filter can be used to receive the DC-component and block the high frequency component. On the other hand, the delay element based method is called delayed signal cancellation (DSC) which is a transformation signals on stationary reference frame. In this approach the three-phase system is delayed by one fourth of period (T/4) at the fundamental frequency. The direct and inverse sequences are then attained by utilising $\alpha\beta$-to-dq transformation.

However, the filter affects the response time of the control system and the quality of the regulator is therefore decreased. When the system requires fast response time, the delay of $T/4$ becomes too long. Hence, a new separate method is introduced in order to support the generator working faster and increase the overall performance.

The three-phase variables of the current, voltage or flux can be considered as the α-axis components of the three rotary vectors $\underline{Z}_a$, $\underline{Z}_b$, $\underline{Z}_c$ (Figure 4). When there is a drop on the mains voltage, the three-phase variables are asymmetrical and the amplitude and the phase shift among $\underline{Z}_a$, $\underline{Z}_b$, $\underline{Z}_c$ are not the same. The three-phase PLL is used to determine the angle of the entire vector. This angle is the same as that of $\underline{Z}_a$. The entire vector lies on the d-axis and its q-component is kept to 0 (Figure 5). The parameters of the controller are calculated under the consideration that the PLL plant is a simple lag (sampling delay) along with an integrating element as shown in Eq. (2) (Kaura and Blasko, 1997).

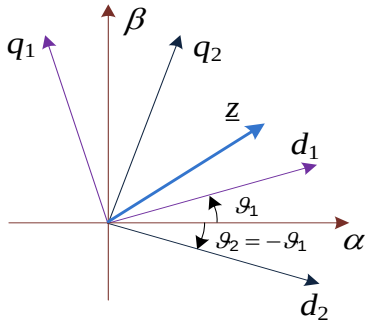

Fig. 3 Representation of a static coordinate system, direct rotation and inverse rotation

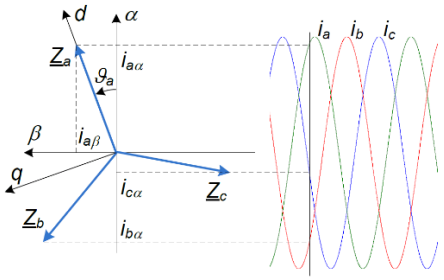

Fig. 4 Representation of three phase variable with three rotating vectors

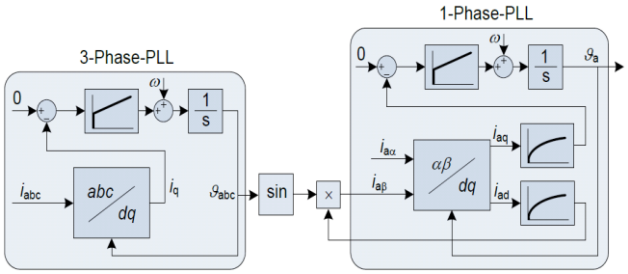

Fig. 5 Determination of $\underline{Z}_a$ with 3-Phase and 1-Phase PLL

$$G_{PLL} = \frac{I_a}{s\left(1+T_{PLL}\ s\right)} \tag{2}$$

The parameters of the PI-controller can be determined according to symmetrical optimum method. With the angle from the 3-phase PLL, the 1-phase PLL determines the β-axis component of the $\underline{Z}_a$. The two first-order filters after the Park transformation determine the dynamic of the PLL (Filho *et al*., 2008). By using the two PLLs, each of vectors $\underline{Z}_a$, $\underline{Z}_b$ or $\underline{Z}_c$ is determined and the direct and inverse components are calculated by the conventional symmetric component transformation. The dq-components of the direct and inverse sequences are obtained by Park transformation.

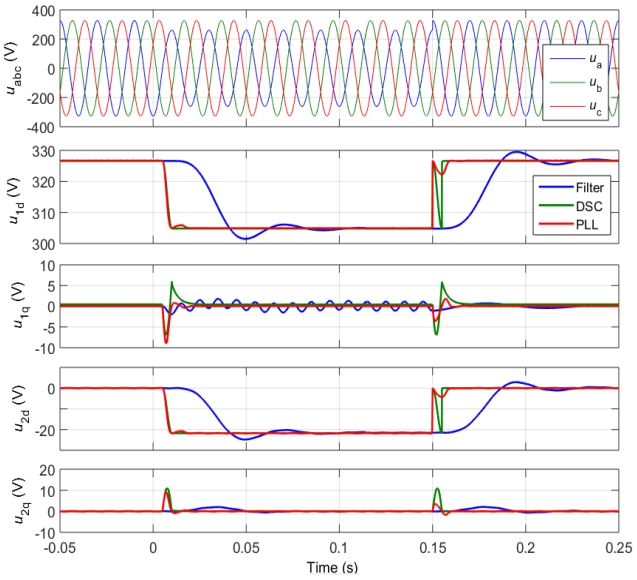

Fig. 6 Comparison of the direct and inverse sequence separation methods

The behaviour of this proposed PLL method is compared with filter and DSC methods (Figure 6). The result is obtained under 20 % 1-phase voltage sag in 150 ms. The response time of the filter method is too long. The DSC method is fast enough but the delay of *T*/4 does not allow the method to work really well. The behaviour of the proposed PLL method is better with very short response time.

2.4 System modelling

2.4.1 Direct system model

Normally, grid-connected controllers often rely on mains voltage and mains frequency as a reference to give active and reactive power characteristics. In case of grid asymmetry, the reference to this voltage component can cause instability for the control system because the voltage component in the rotation coordinate system appears to fluctuate. Obviously, if we convert the three-phase system to two symmetrical systems, we will obtain stable and fully controllable rotational components like the normal state. In order to build a controller in both direct and inverse systems, the grid connection elements need to be modelled. Accordingly, the LC filter circuit and the grid equivalent circuit are modelled according to Figure 7.

Eq. (3, 4, 5) illustrate the voltages after the DC-AC converter and the mains voltage.

$$\underline{u}_{\mathrm{n}} = R_{\mathrm{f}}\,\underline{i}_{\mathrm{n}} + L_{\mathrm{f}}\,\frac{\mathrm{d}\underline{i}_{\mathrm{n}}}{\mathrm{d}t} + \mathrm{j}\,w_{\mathrm{N}}\,L_{\mathrm{f}}\,\underline{i}_{\mathrm{n}} + \underline{u}_{\mathrm{C}} \tag{3}$$

$$\underline{u}_{\mathrm{N}} = R_{\mathrm{N}}\,\underline{i}_{\mathrm{N}} + L_{\mathrm{N}}\,\frac{\mathrm{d}\underline{i}_{\mathrm{N}}}{\mathrm{d}t} + \mathrm{j}\,w_{\mathrm{N}}\,L_{\mathrm{N}}\,\underline{i}_{\mathrm{N}} + \underline{u}_{\mathrm{C}} \tag{4}$$

$$\underline{i}_{\mathrm{C}} = C_{\mathrm{f}}\,\frac{\mathrm{d}\underline{u}_{\mathrm{C}}}{\mathrm{d}t} + \mathrm{j}\,w_{\mathrm{N}}\,C_{\mathrm{f}}\,\underline{u}_{\mathrm{C}} = \underline{i}_{\mathrm{N}} + \underline{i}_{\mathrm{n}} \tag{5}$$

where f, n and N denoting the quantities at the filter, the converter output and at the grid, respectively. The symbols *i*, *u*, and *ω* are the variables for current, voltage and angular velocity, respectively. Since the orientation for the rotation coordinate system *dq* is based on the mains voltage, the mains voltage component is estimated by Eq. (6, 7).

$$u_{\mathrm{Nd}} = \left\|\underline{u}_{\mathrm{N}}\right\| \tag{6}$$

$$u_{\mathrm{Nq}} = 0 \tag{7}$$

Since the voltage drop across the line impedance Z_{N} can be neglected and the voltage across the filter capacitor is considered to be equal to the mains voltage as described by Eq. (8).

$$u_{\mathrm{Cd}} \cong u_{\mathrm{Nd}} \tag{8}$$

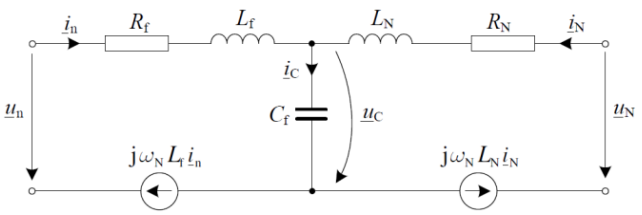

Fig. 7 Equivalent circuit of direct system

With this approximation, expanding the equations (3)-(4), the mains voltage components on the rotating system are determined by Eq. (9, 10).

$$u_{\mathrm{Nd}} = -R_{\mathrm{f}}\,i_{\mathrm{nd}} - L_{\mathrm{f}}\,\frac{\mathrm{d}i_{\mathrm{nd}}}{\mathrm{d}t} + w_{\mathrm{N}}\,L_{\mathrm{f}}\,i_{\mathrm{nq}} + u_{\mathrm{nd}} \tag{9}$$

$$u_{\mathrm{Nq}} = 0 = -R_{\mathrm{f}}\,i_{\mathrm{nq}} - L_{\mathrm{f}}\,\frac{\mathrm{d}i_{\mathrm{nq}}}{\mathrm{d}t} - w_{\mathrm{N}}\,L_{\mathrm{f}}\,i_{\mathrm{nd}} + u_{\mathrm{nq}} \tag{10}$$

Because the phase sequence and rotation direction coincide with the original three-phase system, the model representation of the direct system is exactly the same as described above.

2.4.2 Inverse system model

For the inverse system, the components vary with opposite angular rates. The equivalent circuit is shown as Figure 8. Similar to the implementation for the direct system, the components on the rotation coordinate system for the inverse system are described by Eq. (11, 12).

$$u_{\mathrm{N2d}} = -R_{\mathrm{f}}\,i_{\mathrm{n2d}} - L_{\mathrm{f}}\,\frac{\mathrm{d}i_{\mathrm{n2d}}}{\mathrm{d}t} - w_{\mathrm{N}}\,L_{\mathrm{f}}\,i_{\mathrm{n2q}} + u_{\mathrm{n2d}} \tag{11}$$

$$u_{\mathrm{N2q}} = -R_{\mathrm{f}}\,i_{\mathrm{n2q}} - L_{\mathrm{f}}\,\frac{\mathrm{d}i_{\mathrm{n2q}}}{\mathrm{d}t} + w_{\mathrm{N}}\,L_{\mathrm{f}}\,i_{\mathrm{n2d}} + u_{\mathrm{n2q}} \tag{12}$$

2.4.3 Model of converter and DC-link

The DC-AC converter converts direct current from solar panels to three-phase AC current. There are many methods of performing switching of semiconductor valves. For control purposes, a switch can be considered ideal when ignoring losses. Eq. (13) expresses power on DC-link.

$$p_{\mathrm{DC}} = u_{\mathrm{DC}}\,i_{\mathrm{DCn}} \tag{13}$$

The DC-link model is simplified to a T-circuit (Figure 9) with the capacitor current being the error between the input current from the solar panel current controller and the output current to the DC-AC converter as determined by Eq. (14).

$$i_{\mathrm{DC}}(t) = i_{\mathrm{DCs}}(t) - i_{\mathrm{DCn}}(t) \tag{14}$$

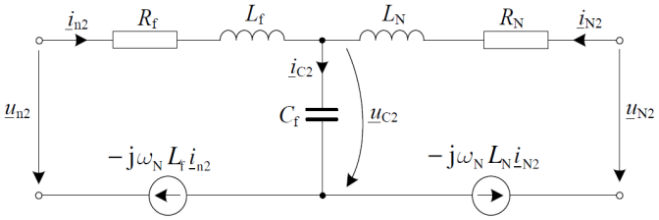

Fig. 8 Equivalent circuit of inverse system

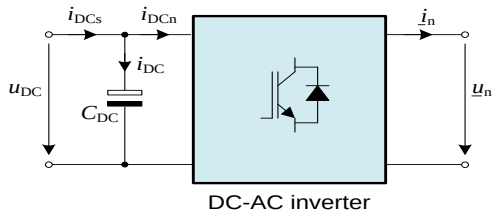

Fig. 9 DC-link equivalent circuit

This current determines the voltage across the capacitor as shown in Eq. (15).

$$u_{DC}(t) = \frac{1}{C_{DC}} \int i_{DC}(t)\mathrm{d}t + u_{DC0} \tag{15}$$

3. Controller construction

Key functions of the DC-AC converter controller are to ensure active power transmission from the panel to the grid, to keep the DC-link voltage stable and to ensure that the output AC voltage coincides with the grid in terms of amplitude and frequency. The mains voltage component needs to be determined to serve the control of the current components corresponding to the active and reactive power. That means the voltage after the DC-AC converter must be in sync with the mains voltage. When the grid fault occurs, the direct component controller still performs the control of the two power components, while the inverse component controller (ICC) performs the asymmetry correction on the grid according to the predefined standards. Because a star-delta transformer (three-phase power transmission system without a neutral wire) is often placed between the generator and the fault, the zero-order component does not directly affect the inverter and can be ignored in the control algorithm. Based on the model of grid-connected control elements, the controller needs to be structured appropriately, ensuring the system's linear operation and fast response time.

3.1 Current control loop

The three-phase current components are converted into components on the rotational system *dq* of the direct and inverse systems based on the rotation angle ϑ_{N1}. The direct system reference currents are generated from the DC voltage and reactive power control loop, while the inverse system reference currents are calculated through predetermined standards.

The controller design is based on the modelling formulas (9) - (12). After Laplace transformation on both sides of the equations, the current components are described as expressed in Eq. (16, 17, 18, 19).

$$i_{n1d}(s) = \left[u_{n1d}(s) - u_{N1d}(s) + w_N L_f i_{n1q}(s)\right] G_{in}(s) \tag{16}$$

$$i_{n1q}(s) = \left[u_{n1q}(s) - w_N L_f i_{n1d}(s)\right] G_{in}(s) \tag{17}$$

$$i_{n2d}(s) = \left[u_{n2d}(s) - u_{N2d}(s) - w_N L_f i_{n2q}(s)\right] G_{in}(s) \tag{18}$$

$$i_{n2q}(s) = \left[u_{n2q}(s) - u_{N2q}(s) + w_N L_f i_{n2d}(s)\right] G_{in}(s) \tag{19}$$

where the relationship between voltage and current is described by Eq. (20).

$$G_{in}(s) = \frac{1}{sL_f + R_f} = \frac{K_{in}}{sT_f + 1} \tag{20}$$

with $K_{in} = 1/R_f$ and $T_f = L_f/R_f$. At the converter, the total time constant component T_t including dead-time, signal measurement, analog-to-digital conversion, and processing time is approximated by a first-order inertial transfer function as shown in Eq. (21).

$$G_{bd}(s) = \frac{1}{sT_t + 1} \tag{21}$$

Thus, inside the system, there exist two first-order inertia transfer functions, fast and slow (T_t << T_f). Applying the modulus optimization criterion, Eq. (22, 23) determine the PI regulator parameters.

$$K_{Pin} = \frac{L_f}{2T_t} \tag{22}$$

$$T_{Iin} = T_f \tag{23}$$

Hence, the current-controlled closed-loop is approximated by Eq. (24).

$$G_{Kin}(s) = \frac{1}{2T_t^2 s^2 + 2T_t s + 1} \cong \frac{1}{2T_t s + 1} \tag{24}$$

The direct and inverse current control loop structure is described in Figure 10.

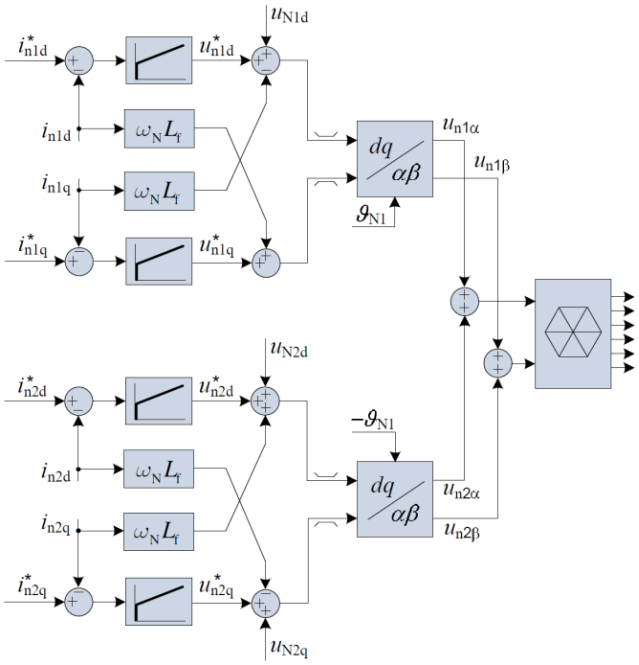

Fig. 10 Structure of the direct and inverse controller

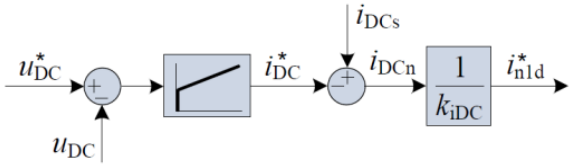

Fig. 11 DC-link equivalent circuit

3.2 DC-link voltage control

The DC-link voltage is determined by capacitance C_{DC} and capacitor current. This constant voltage control means that the capacitor current is zero and the active current to the grid is equal to the current generated by the panels. Applying Laplace transform to formula (15), Eq. (25) shows the relationship of current and voltage on the capacitor.

$$G_{DC}(s) = \frac{u_{DC}(s)}{i_{DC}(s)} = \frac{1}{C_{DC}s} \tag{25}$$

If the losses of the wire impedance and the switching of the semiconductor valve are neglected, the power on the capacitor p_{DC} and the output power p_N are equal. This relationship is represented by Eq. (26).

$$u_{DC}\, i_{DCn} = \frac{3}{2}(u_{N1d} i_{n1d} + u_{N1q} i_{n1q}) \tag{26}$$

Because the control system follows the direct voltage rotation angle, $u_{N1q} = 0$. The current relationship before and after the inverter is shown in Eq. (27, 28).

$$i_{DCn} = k_{iDC}\, i_{n1d} \tag{27}$$

$$k_{iDC} = \frac{3}{2}\frac{u_{N1d}}{u_{DC}} \tag{28}$$

From Equations (14), (25) and (27) the DC voltage controller is represented as Figure 11.

According to (15), the relationship between the input current and the output voltage of the capacitor is an integral block. Combining this relationship with the current-controlled closed-loop transfer function, the PI controller parameters can be determined through the symmetric optimization criterion. Accordingly, Eq. (29, 30) determine the voltage controller parameters.

$$K_{PDC} = \frac{C_{DC}}{4T_t} \tag{29}$$

$$T_{IDC} = 8T_t \tag{30}$$

3.3 Reactive power control

Depending on the load characteristics, the required reactive power is adjusted to reduce line loss and improve the efficiency of real power transmission. On the other hand, for weak power networks, when there is a voltage drop, reactive power contributes to fast grid recovery, ensuring grid connection standards of renewable energy systems. Similar to determining the active power at the system output, the reactive power is calculated by Eq. (31).

$$q_n = \frac{3}{2}(u_{N1q} i_{n1d} - u_{N1d} i_{n1q}) \tag{31}$$

Since the control follows the mains voltage angle, the reactive power is estimated by Eq. (32).

$$q_n = -\frac{3}{2} u_{N1d} i_{n1q} \tag{32}$$

Since then, combined with closed loop current control, the relationship between reactive power and reactive current component is determined by Eq. (33, 34).

$$G_{qn}(s) = \frac{q_n(s)}{i^*_{n1q}(s)} = \frac{K_{qn}}{2T_t s + 1} \tag{33}$$

$$k_{qn} = -\frac{3}{2} u_{N1d} \tag{34}$$

With the requirement that the controller ensures low overshoot and avoids oscillations in the system, the controller parameters can be determined according to the damping optimal criteria. Accordingly, to maintain the standard closed-loop oscillator, an integral control can be used with the gain calculated by Eq. (35).

$$K_{Iqn} = \frac{1}{2T_t K_{qn}} \tag{35}$$

The controller structure is described as Figure 12.

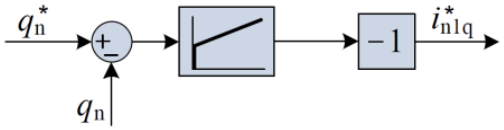

Fig. 12 Reactive power controller

Table 1
System simulation parameters

Parameter	Symbol	Value	Unit
Rated mains voltage	U_N	400	V
Rated output power	P_N	4	kW
Filter inductance	L_f	8	mH
Active power	p_n	3	kW
Reactive power	q_n	1	kVAr
Number of dip phase		2	
Voltage dip level	U_{dip}	35	%
Voltage dip duration	t_{dip}	150	ms

3.4 Inverse system control

When an asymmetric voltage drop occurs, the components of the inverse system appear. The inverse system controller affects the current through a corresponding voltage change. On the basis of purposeful conversion to inverse current, the parameters affected by voltage drop will change in the positive trend and support more stable direct system controller. The inverse control standards corresponding to the reference components are simulated with circuit parameters and operating conditions shown in Table 1. For the case that affects the system the most, this paper only presents the characteristics of the two-phase voltage drop case.

3.4.1 Eliminating current unbalance

For symmetric three-phase load systems, generating a balanced current while asymmetrical voltage maintains thermal equilibrium across the load and across the converter power element. This has real implications for systems that use rotating electrical machines. This control standard is implemented by controlling the inverse current components to zero.

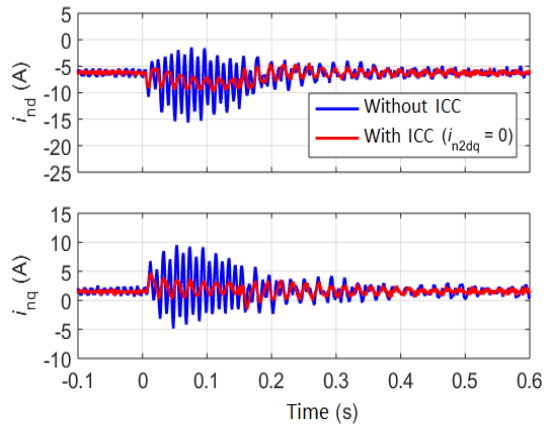

Fig. 13 Filter current components with and without inverse component controller

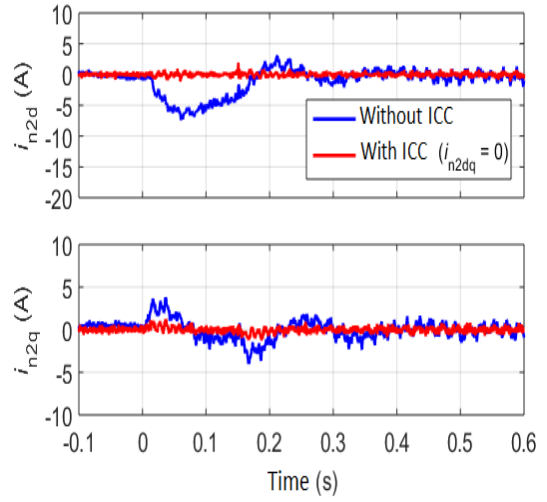

Fig. 14 Inverse current components behaviour with and without their controller

Figures 13 and 14 describe the characteristics of the output current and inverse current components before and after applying the current balance standard for the two-phase voltage drop case. For the current characteristic after the filter (Figure 13), it can be seen that, in the absence of the inverse controller, due to the existence of an inverse current component (Figure 14), there is a large fluctuation in the current characteristic. The large negative current amplitude makes the oscillation amplitude correspondingly large. Vibration frequency can be seen as two times larger than the base frequency (50Hz) (Hunter *et al.*, 2019). This is because the inverse component rotates inversely to the forward component with a rotation angle of $-2\vartheta_1$ (when viewed from the forward *dq* coordinate system) (Figure 3). When comparing the inverse current component on the *d* and *q* axes, it can be seen that the inverse current amplitude in the *d* component is larger than that of the *q* component. This is because the active and reactive power settings are different. According to Table 1, the active power value is three times larger than the reactive power. After applying the inverse controller, simulation results show that, the inverse current components are controlled to zero in order to balance the three-phase current in the grid. Obviously, the current component in both the *d* and *q* axes is zero (Figure 14). Accordingly, at the current output (Figure 13), the component of oscillation at twice the base frequency is absent. The frequency on the current has a 50Hz component with a small amplitude. This is part of the transient characteristic at the beginning and at the end of the fault. With the advantage of the controller as described above, the current unbalance is significantly reduced by 84% compared to the case without the inverse component controller (ICC).

3.4.2 Reducing active power fluctuations

As mentioned in the voltage drop standard, depending on the condition, the direct controller will give priority to active or reactive power generation. In the case of active power generation, the inverse controller needs to reduce the fluctuating state of this power. According to Ferre *et al.* (2011), the active power when there is a grid imbalance fault is described as shown in Eq. (36) consisting of three components.

$$P_N = P_{N0} + P_{N\text{-cos}}\cos(2w_N t) + P_{N\text{-sin}}\sin(2w_N t) \quad (36)$$

where the two components $P_{N\text{-cos}}$ and $P_{N\text{-sin}}$ representing the amplitude of the power oscillation, the component P_{N0} being the stable power when there is no voltage drop. The oscillation components are calculated by Eq. (37, 38).

$$P_{N\text{-cos}} = 3(u_{N1d}i_{N2d} + u_{N1q}i_{N2q} + u_{N2q}i_{N1q} + u_{N2d}i_{N1d})/2 \quad (37)$$

$$P_{N\text{-sin}} = 3(u_{N1d}i_{N2q} - u_{N1q}i_{N2d} + u_{N2q}i_{N1d} - u_{N2d}i_{N1q})/2 \quad (38)$$

To minimize this power fluctuation, the inverse controller needs to drive this oscillating component to zero. With voltage component estimation according to (6) – (7), the inverse controller reference current components are calculated in Eq. (39, 40).

$$i_{n2d} = (-u_{N2q}i_{n1q} - u_{N2d}i_{n1d})/u_{N1d} \quad (39)$$

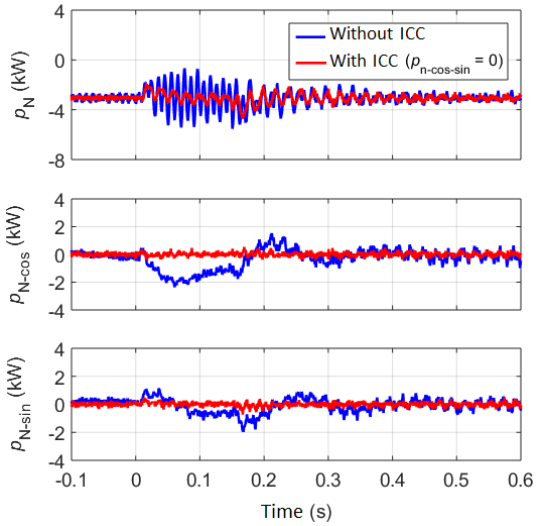

Fig. 15 Active power and its oscillation components

$$i_{n2q} = (-u_{N2q} i_{n1d} + u_{N2d} i_{n1q}) / u_{N1d} \quad (40)$$

Figure 15 shows the simulated performance of the active power stabilization standard with and without an inverse controller. It can be seen that, when a voltage drop occurs, at time t = 0, the $p_{N\text{-}cos}$ and $p_{N\text{-}sin}$ components have increased values. They are the components that cause fluctuations in the active power characteristics. Similar to the characteristic of current, this power in the absence of the inverse controller oscillates with a rather high amplitude as approximately twice as the value of the set power. This amplitude corresponds to the level of voltage drop on the grid side. Since the inverse component is in the opposite direction compared to the forward component, the frequency of oscillation at active power is at 100Hz (Vicuna *et al.*, 2015). With the benefit of the inverse controller, the $p_{N\text{-}cos}$ and $p_{N\text{-}sin}$ components are driven to zero during the fault as shown in the lower two graphs in Figure 15. This helps the real power to significantly reduce fluctuations and bring stable power to the load. With the parameters set for the controller, the oscillation of the active power is significantly reduced to 18 % compared to when the controller is not used.

3.4.3 Reducing reactive power fluctuations

Reactive power plays a role in assisting grid recovery during deep voltage drops. According to Ferre *et al.* (2011), Eq. (41, 42) describe the components of this power with three components.

$$Q_N = Q_{N0} + Q_{N\text{-}cos}\cos(2w_N t) + P_{N\text{-}sin}\sin(2w_N t) \quad (41)$$

where

$$Q_{N\text{-}cos} = 3(u_{N1q} i_{N2d} - u_{N1d} i_{N2q} + u_{N2q} i_{N1d} - u_{N2d} i_{N1q}) / 2$$
$$Q_{N\text{-}sin} = 3(u_{N1q} i_{N2q} + u_{N1d} i_{N2d} - u_{N2q} i_{N1q} - u_{N2d} i_{N1d}) / 2 \quad (42)$$

Similar to the active power case, the inverse controller reference components are determined by Eq. (43, 44).

$$i_{n2d} = (u_{N2q} i_{n1q} + u_{N2d} i_{n1d}) / u_{N1d} \quad (43)$$

$$i_{n2q} = (u_{N2q} i_{n1d} - u_{N2d} i_{n1q}) / u_{N1d} \quad (44)$$

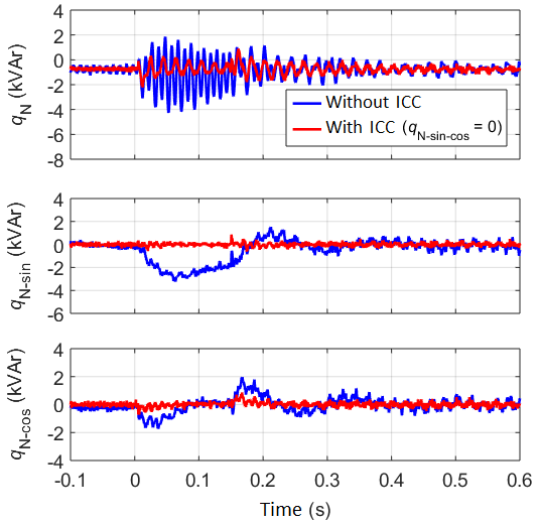

Fig. 16 Reactive power and its oscillation components

Figure 16 shows the control results when there is a voltage drop. Similar to active power control, it can be seen that, when a voltage drop occurs, at time t = 0, the $q_{N\text{-}sin}$ and $q_{N\text{-}cos}$ components have increased values. Although the set value for reactive power is relatively small compared to the actual power, the $q_{N\text{-}sin}$ component has a relatively large value during the voltage drop. From there, it is clear to see the influence of reactive power and the significance of keeping this power component stable in restoring the power grid (Camacho *et al.*, 2013). Similar to the characteristic of active power, in the absence of inverse component controller, the oscillations at reactive power have a rather high amplitude with a frequency at twice the grid frequency (Vicuna *et al.*, 2015). With the benefit of the inverse controller, the $q_{N\text{-}sin}$ and $q_{N\text{-}cos}$ components are driven to zero during the fault as shown in the lower two graphs in Figure 16. This makes real sense when it comes to providing the amount of reactive power needed to support the grid. With the role of inverse controller, the reactive power fluctuation level is reduced up to 14%.

4 Optimal parameter control and experimental results

4.1 Vibration level optimization control (VOC)

With different dip levels and controlled inverse converter current, the vibrations on control variable (filter current, active and reactive powers) are changed. That means it exists a curve which corresponds to a dip level, a value of inverse component current gives a minimum sum of above vibrations. In order to compare variables with different units, their per-unit values are considered.

According to section 3.4, with different voltage drops, the values of the inverse components vary. This study found that, at each voltage drop, for the sum of the inverse components as the filter current varies, there exists a minimum point. At this position, the combined oscillations of the important quantities in the system are lowest. It can be seen that, if we let the system work at this point, the

quality of the inverter or the vibration level (VBL) will be optimal.

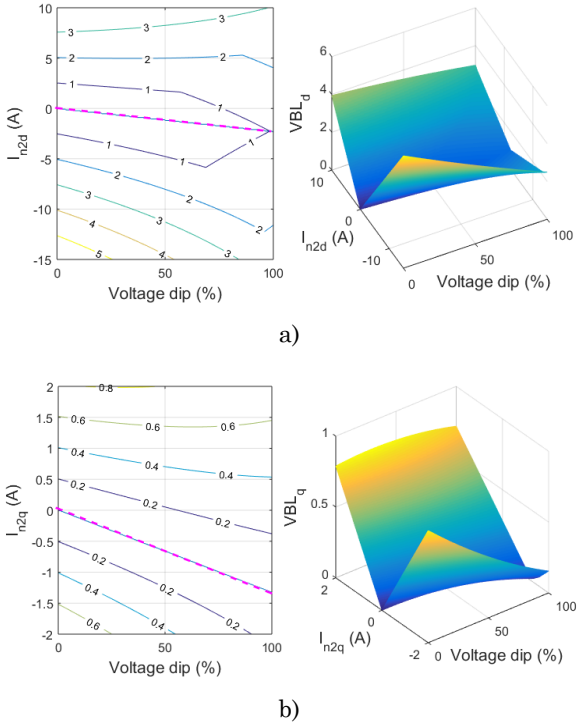

Fig. 17 Optimal reference current trajectory for the *d* and *q*-component of the inverse controller

Figure 17 shows the shape of vibration with different values of inverse filter current and voltage dip. The dashed line represents the optimal operating points of the reference current on the inverse controller.

Accordingly, from the left characteristic, corresponding to a certain voltage drop, it is possible to determine the optimal set value for the reference currents i_{n2d} and i_{n2q}. The voltage drop level can be determined through the PLL method as described in section 2.3. To calculate the reference current component as shown in Figure 17, the table lookup method can be used rather than direct calculation from the system model.

4.2 Experimental results

The results of applying the control algorithm are tested through an experimental test rig. The model is built with the same parameters as the simulation for easy comparison and evaluation. The test rig, includes a computer that collects and determines control parameters, a dedicated controller dSPACE DS1104.

A frequency converter is operated on the vector space principle with some additional elements such as filter coils, capacitors, DC overvoltage protectors. For the experimental investigations under voltage dip, an AC voltage source SW 5250A (ELGAR) is utilised. The power source can generate various voltage profiles with different voltage levels for each single phase. The technical parameters of the voltage source are provided in Table 2.

Table 2
Parameters of SW 5250A AC voltage generator

Variable	Value	Unit
Power (3 phases)	5250	VA
Current per phase	13/6.5	A
AC or DC Voltage (per phase)	135/270	Vrms
Frequency range (DC, AC)	0 - 6	kHz

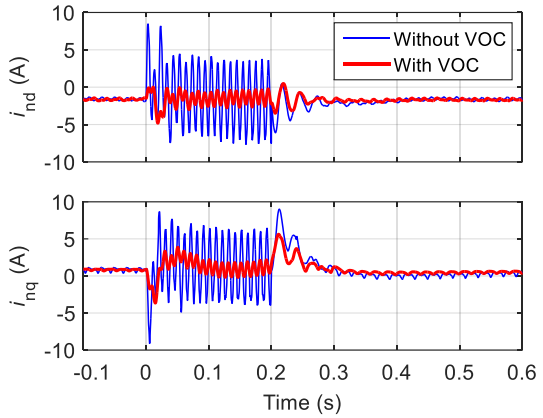

Fig. 18 Performance of the current components at the filter

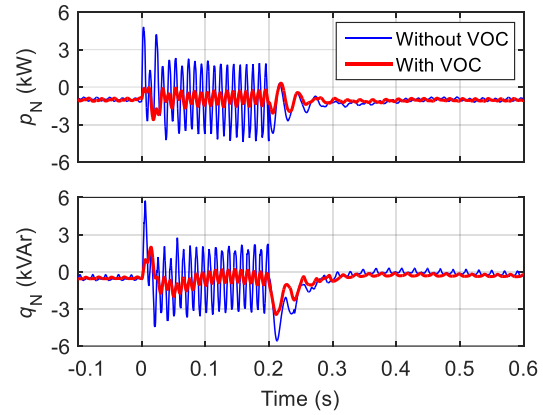

Fig. 19 Performance of active and reactive power at the grid

The performance of the system was investigated under operating parameters described in Table 3. Accordingly, the system is controlled in the event of a grid fault lasting 200ms and a voltage drop of 20%. During the voltage drop, the active and reactive power components remain unchanged at 1kW and 0.5kVAr, respectively. This system is tested in case the grid frequency is 50Hz. The above vibration optimal control (VOC) were applied for two phase asymmetrical voltage dip cases.

Table 3
Operating parameters of test rig

Variable	**Value**	**Unit**
Nominal voltage	400	V
Dip level	20	%
Dip period	200	ms
Dip frequency	50	Hz
Active power	1	kW
Reactive power	0.5	kVAr

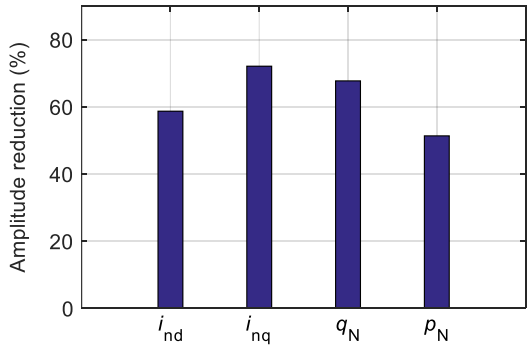

Fig. 20 The oscillation reduction at the parameters when applying the optimal controller

Figures 18 and 19 show the characteristics of the current and power parameters before and after using the optimal parameter controller. Accordingly, the variation of the quantities is significantly reduced when the controller is applied (Camacho *et al*., 2013). As can be seen, there is a similarity between simulation and experimental results. In particular, the unstable variation of the power and current values is greatly improved. This properly reflects the characteristics of symmetrical components affecting the quality of output quantities on the grid. In more detail, the transient variation at the beginning and end of the fault is dramatically reduced, both in current and power characteristics. During oscillation, a frequency component being equal to twice the base frequency still exists (Castilla *et al*., 2010). This is because there is an inverse component in the system. Thanks to the above optimal parameter controller, the output oscillation components are significantly reduced. The oscillation reduction is shown in Figure 20. The oscillation reduction of the current can be up to 28%. As a result, the power output parameter also achieves a clear reduction, by 68%.

5. Conclusions

Energy plays a strategic role in the socio-economic development of the country. The renewable energy system actively contributes to the protection of the natural environment while maintaining energy security. Because this energy component accounts for a large proportion, ensuring system safety in the event of a power grid failure plays a very important role in maintaining the stability of the transmission and distribution system.

This paper proposes a new method to separate symmetrical components in the power grid when there is a voltage drop. Since then, the symmetrical components are independently controlled and improve the quality of the three-phase converter operation. The simulation results show that, by independently controlling the direct and inverse symmetrical components, fluctuations in the load current or power components can be reduced by up to 86%. This also shows accurate modelling results of the system in setting controller parameters.

The research presented in the paper also demonstrates the successful development of an experimental model to verify the above results. Control standards can be combined to minimize simultaneous effects on the generator system and the load when a voltage drop occurs. A generator that produces a voltage drop is used to test the actual properties. The result of the optimal control algorithm on the basis of control according to the characteristic, at which the effect of voltage drop on the system is lowest, is verified. System quality is significantly increased by up to 72% compared to when the inverse component controller is not used.

The research results in the article are not only applied in solar power systems in particular but also in renewable energy generation systems in general. The results presented above are the methodological basis for controlling the connection of the power generation system and restoring the weak power grid.

Funding: The author received no financial support for the research, authorship, and/or publication of this article.

Conflicts of Interest: The authors declare no conflict of interest.

References

Alepuz, S., Busquets, S., Bordonau, J., Pontt, J., Silva, C., & Rodriguez, J. (2007). Fast on-line symmetrical components separation method for synchronization and control purposes in three phase distributed power generation systems. *European Conference on Power Electronics and Applications*, pp. 1-10. DOI: 10.1109/EPE.2007.4417343

Almeida, P. M., Monteiro, K. M., Barbosa, P. G., Duarte J. L., & Ribeiro, P. F. (2016). Improvement of PV grid-tied inverters operation under asymmetrical fault conditions, *Solar Energy*, 133, 363-371. https://doi.org/10.1016/j.solener.2016.04.015.

Arrillaga, J., Bollen, M. H. J., & Watson, N. R. (2000). Power quality following deregulation. *Proceedings of the IEEE*, 88, 246-261. DOI: 10.1109/5.824002.

Banu, I. & Istrate, M. (2014). Study on Three-Phase Photovoltaic Systems under Grid Faults. *International Conference and Exposition on Electrical and Power Engineering* (*EPE*). Doi: 10.1109/ICEPE.2014.6970086.

Camacho, A., Castilla, M., Miret, J., Vasquez, J. C. and Alarcon-Gallo, E. (2013). Flexible Voltage Support Control for Three-Phase Distributed Generation Inverters Under Grid Fault. *IEEE Transactions on Industrial Electronics*, 60(4), 1429-1441. doi: 10.1109/TIE.2012.2185016.

Castilla, M., Miret, J., Sosa, J. L., Matas, J. & Vicuña, L. G. d. (2010). Grid-Fault Control Scheme for Three-Phase Photovoltaic Inverters With Adjustable Power Quality Characteristics. *IEEE Transactions on Power Electronics*, 25(12), 2930-2940. doi: 10.1109/TPEL.2010.2070081.

Chen, M., Afridi, K. K. & Perreault, D. J. (2015). A Multilevel Energy Buffer and Voltage Modulator for Grid-Interfaced Microinverters," in IEEE Transactions on Power Electronics, 30(3), 1203-1219. doi: 10.1109/TPEL.2014.2320965.

Coppola, M., Napoli, F. Di, Guerriero, P., Iannuzzi, D., Daliento, S. & Pizzo, A. D. (2016). An FPGA-Based Advanced Control Strategy of a Grid-Tied PV CHB Inverter. *IEEE Transactions on Power Electronics*. 31(1), 806-816. doi: 10.1109/TPEL.2015.2405416.

Ding, G., Gao, F., Tian, H. & Ma, C. *et al*. (2016). Adaptive DC-Link Voltage Control of Two-Stage Photovoltaic Inverter During Low Voltage Ride-Through Operation. *IEEE Transactions on Power Electronics*, 31(6), 4182-4194. doi: 10.1109/TPEL.2015.2469603.

Dousoky, G. M., Ahmed, E. M. & Shoyama, M. (2013). MPPT schemes for single-stage three-phase grid-connected photovoltaic voltage-source inverters. *IEEE International Conference on Industrial Technology* (*ICIT*). 600-605, doi: 10.1109/ICIT.2013.6505739.

Erlich, I., Winter, W., & Dittrich, A. (2006). Advanced grid requirements for the integration of wind turbines into the

German transmission system. *IEEE Power Engineering Society General Meeting*, 1-7. DOI: 10.1109/PES.2006.1709340

Ferre, A. J., Bellmunt, O. G., Green, T. C., & Sanchez, D. E. S. (2011). Current control reference calculation issues for the operation of renewable source grid interface VSCs under unbalanced voltage sags. *IEEE Trans. on Power Electronics*, 26(12), 3744-3753. DOI: 10.1109/TPEL.2011.2167761

Filho, R. M. S., Seixas, P. F., Cortizo, P. C., Torres, L. A. B., & Souza, A. F. (2008). Comparison of Three Single-Phase PLL Algorithms for UPS Applications, *IEEE Transactions on Industrial Electronics* , 55, 2923-2932. DOI: 10.1109/TIE.2008.924205.

Gagrica, O., Nguyen, P. H., Kling, W. L. & Uhl, T. (2015). Microinverter Curtailment Strategy for Increasing Photovoltaic Penetration in Low-Voltage Networks. *IEEE Transactions on Sustainable Energy*, 6(2), 369-379. doi: 10.1109/TSTE.2014.2379918.

Hajizadeh, A., & Golkar, M. A. (2011). Control of photovoltaic power generation system during unbalanced grid voltage sag conditions. *21st International Conference on Electricity Distribution*, Paper no. 0615, Frankfurt.

Hunter, G., Riedemann, J., & Andrade, I., *et al.* (2019). Power control of a grid-connected PV system during asymmetrical voltage faults. *Electr Eng,* 101, 239–250. https://doi.org/10.1007/s00202-019-00769-x

Kaura, V., & Blasko, V. (1997). Operation of a phase locked loop system under distorted utility conditions, *IEEE Transactions on Industry Applications*, 33, 58-63. DOI: 10.1109/28.567077.

Kim, Y., Ji, Y., Kim, J., Jung, Y. & Won, C. (2013). A New Control Strategy for Improving Weighted Efficiency in Photovoltaic AC Module-Type Interleaved Flyback Inverters. *IEEE Transactions on Power Electronics*, 28(6), 2688-2699. doi: 10.1109/TPEL.2012.2226753.

Kjaer, S. B., Pedersen, J. K., & Blaabjerg, F. (2005). A review of single-phase grid-connected inverters for photovoltaic modules. *IEEE Transactions on Industry Applications*, 41(5), 1292-1306. DOI: 10.1109/TIA.2005.853371

Kyritsis, A. C., Tatakis, E. C. & Papanikolaou, N. P. (2008). Optimum Design of the Current-Source Flyback Inverter for Decentralized Grid-Connected Photovoltaic Systems. *IEEE Transactions on Energy Conversion*, 23(1), 281-293. doi: 10.1109/TEC.2007.895854.

Li, H., Xu, Y., Adhikari, S., Rizy, D. T., Li, F. & Irminger, P. (2012). Real and reactive power control of a three-phase single-stage PV system and PV voltage stability. *IEEE Power and Energy Society General Meeting*. 1-8. doi: 10.1109/PESGM.2012.6343965.

Lin, X., Han, Y., Yang, P., Wang, C. & Xiong, J. (2018). Low-Voltage Ride-Through Techniques for Two-Stage Photovoltaic System under Unbalanced Grid Voltage Sag Conditions. *IEEE 4th Southern Power Electronics Conference* (*SPEC*). 1-8. doi: 10.1109/SPEC.2018.8636016.

Lodh, T. & Agarwal, V. (2016). Single stage multi-port Flyback type solar PV module integrated micro-inverter with battery backup. *IEEE International Conference on Power Electronics, Drives and Energy Systems* (*PEDES*), 1-6, doi: 10.1109/PEDES.2016.7914430.

Meneses, D., García, O., Alou, P., Oliver, J. A. & Cobos, J. A. (2015). Grid-Connected Forward Microinverter With Primary-Parallel Secondary-Series Transformer. *IEEE Transactions on Power Electronics*, 30(9), 4819-4830. doi: 10.1109/TPEL.2014.2365760.

Miret, J., Castilla, M., Camacho, A., Vicuña, L. G. d. & Matas, J. (2012). Control Scheme for Photovoltaic Three-Phase Inverters to Minimize Peak Currents During Unbalanced Grid-Voltage Sags. *IEEE Transactions on Power Electronics*. 27(10), 4262-4271. doi: 10.1109/TPEL.2012.2191306.

Moghadasi, A., Sargolzaei, A., Moghaddami, M., Sarwat, A. I. & Yen, K. (2017). Active and reactive power control method for three-phase PV module-integrated converter based on a single-stage inverter. *IEEE Applied Power Electronics Conference and Exposition* (*APEC*). 1357-1362, doi: 10.1109/APEC.2017.7930873.

Mohanty, E., Swain, R., Pany, S. S., Sahoo, S., Behera, S. S. & Panigrahi, B. K. (2019) Detection of Symmetrical and Unsymmetrical Fault in a PV Connected Power System. *3rd International Conference on Computing Methodologies and Communication* (*ICCMC*), 251-254. doi: 10.1109/ICCMC.2019.8819661.

Nanakos, A. C., Tatakis, E. C. & Papanikolaou, N. P. (2012). A Weighted-Efficiency-Oriented Design Methodology of Flyback Inverter for AC Photovoltaic Modules. *IEEE Transactions on Power Electronics*, 27(7), 3221-3233. doi: 10.1109/TPEL.2011.2182211.

Omar, M.A. and Mahmoud, M.M. (2021). Improvement Approach for Matching PV-array and Inverter of Grid Connected PV Systems Verified by a Case Study. *International Journal of Renewable Energy Development*, 10(4), 687-697. https://doi.org/10.14710/ijred.2021.3608.

Prakash, S. L., Arutchelvi, M. & Sharon, S. S. (2015). Simulation and performance analysis of MPPT for single stage PV grid connected system. *IEEE 9th International Conference on Intelligent Systems and Control* (*ISCO*), 1-6, doi: 10.1109/ISCO.2015.7282391.

Premkumar, M., Karthick, K and Sowmya, R. (2018a). A Review on Solar PV Based Grid Connected Microinverter Control Schemes and Topologies. Int. Journal of Renewable Energy Development, 7(2), 171-182. https://doi.org/10.14710/ijred.7.2.171-182

Premkumar, M., Sumithira, R., & Sowmya, R. (2018b). Modelling and Implementation of Cascaded Multilevel Inverter as Solar PV Based Microinverter Using FPGA. International Journal of Intelligent Engineering and Systems. 11, 18-27.doi: 10.22266/ijies2018.0430.03.

Saccomando, G., & Svensson, J. (2001). Transient operation of grid-connected voltage source converter under unbalanced voltage conditions. *IEEE Industry Applications Conference, 36th IAS Annual Meeting*, 2419-2424. DOI: 10.1109/IAS.2001.955960.

Sahu, P. K., Shaw, P. & Maity, S. 2015). Modeling and control of grid-connected DC/AC converters for single-phase micro-inverter application," *Annual IEEE India Conference* (*INDICON*), 1-6, doi: 10.1109/INDICON.2015.7443537.

Shao, R., Wei, R. & Chang, L. (2014). A multi-stage MPPT algorithm for PV systems based on golden section search method. *IEEE Applied Power Electronics Conference and Exposition* (*APEC*). 676-683. doi: 10.1109/APEC.2014.6803381.

Sosa, J. L., Castilla, M., Miret, J., Matas, J. & Al-Turki, Y. A. (2016). Control Strategy to Maximize the Power Capability of PV Three-Phase Inverters During Voltage Sags. *IEEE Transactions on Power Electronics*, 31(4), 3314-3323. doi: 10.1109/TPEL.2015.2451674.

Tekpeti, B., Kang, X., Kheshti, M. (2017). Particular PV grid-connected system under symmetrical and asymmetrical faults analysis. *IEEE Electrical Power and Energy Conference* (*EPEC*). Doi:10.1109/EPEC.2017.8286146.

Vicuna, L., Hoz, J., Miret, J., Camacho, A. & Castilla, M. (2015). Reactive current injection protocol for low-power rating distributed generation sources under voltage sags. *IET Power Electronics*. 8. Doi:10.1049/iet-pel.2014.0593.

Yang, Y., Blaabjerg, F., & Wang, H.. (2014). Low voltage ride-through of single-phase transformerless photovoltaic inverters. *IEEE Transactions on Industry Applications*, 50(3), 1942 - 1952. DOI: 10.1109/TIA.2013.228296.

Yashi, S., Ikhlaq, H., Bhim, S., & Sukumar, M. (2017). Single-Phase Solar Grid Interfaced System with Active Filtering Using ALCF Based Control Scheme. *IET Generation, Transmission and Distribution*. 11(8). Doi: 10.1049/iet-gtd.2016.1392.

Wang, X. B., Yang, Z. X., Fan, B. & Xu, W. (2015). Control Strategy of Three-Phase Photovoltaic Inverter under Low-Voltage Ride-Through Condition. *Mathematical Problems in Engineering*. 1, 1-23. Doi: 10.1155/2015/790584.

Zapata, J. W., Kouro, S., Aguirre, M. & Meynard, T. (2015). Model predictive control of interleaved dc-dc stage for photovoltaic

microconverters. *41st Annual Conference of the IEEE Industrial Electronics Society*. 4311-4316. doi: 10.1109/IECON.2015.7392771.

Zhang, J., Huang, X., Wu, X. & Qian, Z. (2010). A High Efficiency Flyback Converter With New Active Clamp Technique. *IEEE Transactions on Power Electronics*, 25(7), 1775-1785. doi: 10.1109/TPEL.2010.2042302.

Zhu, G., Ruan, X., Zhang, L. & Wang, X. (2015). On the Reduction of Second Harmonic Current and Improvement of Dynamic Response for Two-Stage Single-Phase Inverter. *IEEE Transactions on Power Electronics*, 30(2), 1028-1041. doi: 10.1109/TPEL.2014.2307092.